Pergamon

Int. J. Heat Mass Transfer. Vol. 37, No. 10, pp. 1535–1543, 1994

0017-9310/94 $7.00 + 0.00

0017-9310(93)E0089-Y

A two-dimensional model of the chemical vapor deposition of silicon nitride in a low-pressure hot-wall reactor including multicomponent diffusion

G. EVANS
Sandia National Laboratories, Livermore, CA 94550, U.S.A.

and

R. GREIF
Mechanical Engineering Department, University of California, Berkeley, CA 94720, U.S.A.

(*Received* 17 *February* 1993 *and in final form* 9 *November* 1993)

Abstract—A multidimensional model has been developed and applied to simulate the chemical vapor deposition (CVD) of silicon nitride from silicon tetrafluoride and ammonia in a low-pressure hot-wall reactor. The purpose of this work is to evaluate the effects of gas-phase transport and reactant depletion on the uniformity and rate of deposition of silicon nitride by CVD in order to provide a basis for reactor scaling and process control. Two irreversible surface reactions are used to model the deposition chemistry. Diffusion is shown to be important relative to convection in transporting gas-phase reactants to the surface where the chemical reactions occur. Reactant depletion also has a significant impact on the deposition. Multicomponent diffusion of the five reacting species is studied by solving the Stefan–Maxwell equations; the results are compared with those obtained using the simpler mixture-averaged approximation to multicomponent diffusion.

INTRODUCTION

THE CHEMICAL vapor deposition (CVD) process is used widely for producing thin layers of materials in the fabrication of microelectronic devices. It is also used to apply coatings on materials for a variety of purposes such as protection of the base material from oxidation and wear. A process for applying silicon nitride coatings on graphite substrates has been studied experimentally by Lee *et al.* [1] at the United Technologies Research Center (UTRC). The UTRC process occurs in a hot-wall (1600–1800 K), low-pressure (1–5 Torr) reactor. Reactants silicon tetrafluoride (SiF_4) and ammonia (NH_3) enter one end of the reactor through a water-cooled coannular injector. Reactions take place on the surfaces of the parts and the reactor, depositing silicon nitride (Si_3N_4) and releasing hydrogen fluoride (HF) into the gas mixture. A competing surface reaction is the decomposition of NH_3 into N_2 and H_2. As the gas-phase mixture flows downstream in the reactor, SiF_4 and NH_3 are depleted and HF, N_2, and H_2 accumulate. Equilibrium calculations [2] have shown that Si_3N_4 is not stable at the process conditions and gas-phase chemistry has been determined to be negligible; thus, surface chemical kinetics and gas-phase transport play crucial roles in the deposition process.

In some CVD processes the reactants flow with a chemically inert diluent gas. Under these conditions the effects of the deposition process on the momentum and energy transport are negligible, and the distributions of species are determined by solving species mass balances, given the fluid flow and temperature fields. In the Si_3N_4 process considered here, there is no diluent; thus the species transport and surface reactions are coupled to the mass and momentum transport. In general, the energy release by the surface reactions would also affect the energy transport through the thermal boundary conditions. The emphasis in this work is on mass transport and we restrict the study to isothermal flow.

In general, complex and highly variable geometries are involved due to the diverse array of parts that require coating. The low pressure aspects of the process reduce, but do not eliminate, fluid mechanical effects associated with the complex shapes and multiple flow paths. The utilization of models allows the interactions of transport processes and surface chemistry to be studied and provides the basis for scaling the Si_3N_4 process to coat large and complex shaped parts. The model developed to study the UTRC process incorporates the effects of two-dimensional gas flow, surface chemical kinetics, and multicomponent diffusive transport in complex geometries using a gen-

NOMENCLATURE

D^*	tube diameter [cm]
D_{km}	mixture-averaged diffusion coefficient for species k in the mixture, or coefficient of part of multicomponent diffusion formulation, see equations (6), (8)
Da_{km_α}	Damkohler numbers for surface reaction α and species k in the mixture m
$\mathfrak{D}_{ik}$	binary diffusion coefficient for species i and k
Fr	Froude number, $u^{*2}_{\text{ref}}/(g^*D^*)$
g	acceleration of gravity
$\mathbf{j}^c_k$	ordinary mass diffusion flux vector of species k
K	total number of gas phase species
L^*	tube length [cm]
M	molecular weight of mixture
M_i	molecular weight of species i
$\mathbf{n}$	outward unit normal vector at reacting surface
P	pressure
p_m	dynamic pressure
Q^*	dimensional flow rate in sccm [standard cm^3 min^{-1})
R	gas constant
Re	Reynolds number, $\rho^*_{\text{ref}}u^*_{\text{ref}}D^*/\mu^*_{\text{ref}}$
r	radial coordinate
r_α	reaction rate of surface reaction α
Sc_{km}	Schmidt number for species k in the mixture, $\nu^*_{\text{ref}}/D^*_{km\,\text{ref}}$
T	temperature
t	time
u	axial velocity
v	radial velocity
x	axial coordinate
X_i	mole fraction of species i
Y_k	mass fraction of species k.

Greek symbols

ε	temperature ratio, $(T^*_{\max}-T^*_{\text{ref}})/T^*_{\text{ref}}$
μ	dynamic viscosity
ν	kinematic viscosity
$\rho_k\mathbf{v}_k$	mass flux vector of species k
ρ	density.

Subscripts and superscripts

km	refers to species k in the mixture m
ref	reference quantity
s	evaluated at reacting surface
x	x component
*	dimensional quantity.

eralized nonorthogonal coordinate system. An extensive study has been carried out and results from the model have been used to provide design information for scaling the process from a laboratory facility to a production reactor for coating a diverse array of complex shaped parts.

In the current study the geometry is simplified to facilitate the study of the fundamental physical and chemical processes. Specifically, the geometries of the reactor inlet region and the part are replaced by a simple tube with deposition occurring on the tube wall. Since the Si_3N_4 process occurs in a hot wall reactor with the bulk of the deposition occurring on the reactor wall, this simplification is not unreasonable. The reactor model consists of two regions: an upstream region where no surface reactions occur and a downstream region with surface chemistry (cf. Fig. 1). It may be desirable in certain situations to avoid deposition on the reactor wall in the upstream portion of the reactor and thus conserve reactants for use in the region where the part is located. Here, the nonreacting region is included to study the effects of species diffusion on the transport processes near the leading edge of the deposition region. The model assumes premixed reactants at the inlet.

We use the model to study the effects of the process parameters on the deposition rate and uniformity. The relative effects of convection and diffusion are determined by varying the Reynolds number, i.e. flow rate; the relative effects of surface chemistry and diffusion are determined by varying the surface Damkohler numbers, i.e. temperature and molar ratio of reactants. Calculations have been carried out using both the approximate mixture-averaged formulation for species diffusion as well as the full multicomponent formulation. Depletion of reactants in the streamwise direction and diffusional limitations associated with transport through the developing concentration boundary layers are primarily responsible for nonuniform deposition.

ANALYSIS

The dimensionless equations for mixture mass and momentum and species mass conservation are given (in cylindrical coordinates) by:

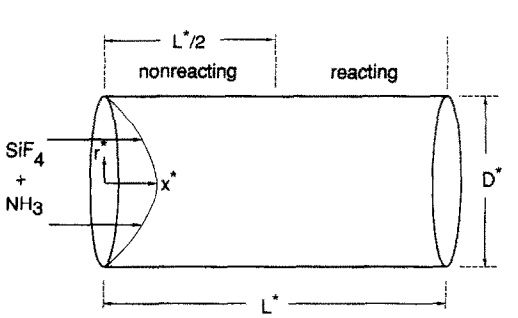

FIG. 1. Problem description.

$$\frac{\partial \rho}{\partial t}+\frac{1}{r}\frac{\partial(r\rho v)}{\partial r}+\frac{\partial(\rho u)}{\partial x}=0 \tag{1}$$

$$\begin{aligned}\frac{\partial(\rho u)}{\partial t}&+\frac{1}{r}\frac{\partial}{\partial r}\left(r\rho vu-\frac{r\mu}{Re}\frac{\partial u}{\partial r}\right)\\&+\frac{\partial}{\partial x}\left(\rho uu-\frac{\mu}{Re}\frac{\partial u}{\partial x}\right)=-\frac{\partial p_m}{\partial x}\\&+\frac{1}{Fr}\frac{g_x(\rho-1)}{g}+\frac{1}{Re}\frac{1}{r}\frac{\partial}{\partial r}\left(r\mu\frac{\partial v}{\partial x}\right)\\&+\frac{1}{Re}\frac{\partial}{\partial x}\left\{\mu\frac{\partial u}{\partial x}-\frac{2\mu}{3}\left[\frac{1}{r}\frac{\partial(rv)}{\partial r}+\frac{\partial u}{\partial x}\right]\right\}\end{aligned} \tag{2}$$

$$\begin{aligned}\frac{\partial(\rho v)}{\partial t}&+\frac{1}{r}\frac{\partial}{\partial r}\left(r\rho vv-\frac{r\mu}{Re}\frac{\partial v}{\partial r}\right)\\&+\frac{\partial}{\partial x}\left(\rho uv-\frac{\mu}{Re}\frac{\partial v}{\partial x}\right)=-\frac{\partial p_m}{\partial r}\\&+\frac{1}{Fr}\frac{g_r(\rho-1)}{g}+\frac{1}{Re}\frac{1}{r}\\&\times\frac{\partial}{\partial r}\left\{r\mu\left[\frac{\partial v}{\partial r}-\frac{2}{3}\left(\frac{1}{r}\frac{\partial(rv)}{\partial r}+\frac{\partial u}{\partial x}\right)\right]\right\}\\&-\frac{1}{Re}\frac{\mu}{r}\left\{\frac{2v}{r}-\frac{2}{3}\left[\frac{1}{r}\frac{\partial(rv)}{\partial r}+\frac{\partial u}{\partial x}\right]\right\}\\&+\frac{1}{Re}\frac{\partial}{\partial x}\left(\mu\frac{\partial u}{\partial r}\right)\end{aligned} \tag{3}$$

$$\begin{aligned}\frac{\partial(\rho Y_k)}{\partial t}&+\frac{\partial}{\partial x}\left(\rho uY_k+\frac{j^c_{k_x}}{Re\cdot Sc_{km}}\right)\\&+\frac{1}{r}\frac{\partial}{\partial r}\left(r\rho vY_k+\frac{rj^c_{k_r}}{Re\cdot Sc_{km}}\right)=0,\\&\qquad k=1,\ldots,(K-1)\end{aligned} \tag{4}$$

where $j^c_{k_x}$ and $j^c_{k_r}$ are the components of the ordinary mass diffusion flux vector $\mathbf{j}^c_k$ which (for multicomponent diffusion) can be expressed as (Kleijn [3]):

$$\mathbf{j}^c_k/j^{c^*}_{k\,\mathrm{ref}}=\mathbf{j}^c_k=-\frac{\rho D_{km}}{M}\nabla(Y_kM)+D_{km}Y_kM\sum_{i\neq k}\frac{\mathbf{j}^c_i}{M_i\mathfrak{D}_{ik}} \tag{5}$$

where

$$D_{km}=\left[\sum_{i\neq k}X_i/\mathfrak{D}_{ik}\right]^{-1} \tag{6}$$

or (for the mixture-averaged approximation to the ordinary diffusion):

$$\mathbf{j}^{c^*}_k/j^{c^*}_{k\,\mathrm{ref}}=\mathbf{j}^c_k=-\frac{\rho D_{km}}{M}\nabla(Y_kM) \tag{7}$$

where (Curtiss and Hirschfelder [4], Kee *et al.* [5])

$$D_{km}=\frac{1-Y_k}{\sum_{i\neq k}X_i/\mathfrak{D}_{ik}}. \tag{8}$$

The mass source terms have been deleted from equations (4) since homogeneous chemical reactions are not considered in the present study. The K species mass fractions, Y_k, are determined by solving the $K-1$ species conservation equations (4) along with the requirement that $\Sigma_1^K Y_k=1$. Reference quantities used to nondimensionalize the above equations are: tube diameter, D^*; average velocity of mixture at tube inlet ($x=0$), $u^*_{\mathrm{ref}}=4Q^*_{\mathrm{ref}}M^*_{\mathrm{ref}}/(\rho^*_{\mathrm{ref}}\pi D^{*2})$; species k mass diffusion flux, $j^{c^*}_{k\,\mathrm{ref}}=\rho^*_{\mathrm{ref}}D^*_{km\,\mathrm{ref}}/D^*$; mixture density, $\rho^*_{\mathrm{ref}}=P^*M^*_{\mathrm{ref}}/(R^*T^*_{\mathrm{ref}})$; and mixture molecular weight,

$$M^*_{\mathrm{ref}}=X_{SiF_4}|_{(x=0^-)}\cdot M^*_{SiF_4}+X_{NH_3}|_{(x=0^-)}\cdot M^*_{NH_3}$$

where $D^*_{km\,\mathrm{ref}}$ is the diffusion coefficient from either equation (6) or (8), evaluated at the reference conditions: P^*, T^*_{ref}, $X_{SiF_4}|_{(x=0^-)}$, and $X_{NH_3}|_{(x=0^-)}$.

For numerical solution purposes, equations (4) are rearranged into the following form:

$$\begin{aligned}\frac{\partial(\rho Y_k)}{\partial t}&+\frac{\partial}{\partial x}\left(\rho uY_k-\frac{\rho D_{km}}{Re\cdot Sc_{km}}\frac{\partial Y_k}{\partial x}\right)\\&+\frac{1}{r}\frac{\partial}{\partial r}\left(r\rho vY_k-\frac{r\rho D_{km}}{Re\cdot Sc_{km}}\frac{\partial Y_k}{\partial r}\right)\\&=\frac{\partial}{\partial x}\left[\frac{Y_kD_{km}}{Re\cdot Sc_{km}}\left(\frac{\rho}{M}\frac{\partial M}{\partial x}-M\sum_{i\neq k}\frac{j^c_{i_x}}{M_i\mathfrak{D}_{ik}}\right)\right]\\&+\frac{1}{r}\frac{\partial}{\partial r}\left[\frac{rY_kD_{km}}{Re\cdot Sc_{km}}\left(\frac{\rho}{M}\frac{\partial M}{\partial r}\right.\right.\\&\left.\left.-M\sum_{i\neq k}\frac{j^c_{i_r}}{M_i\mathfrak{D}_{ik}}\right)\right],\quad k=1,\ldots,(K-1).\end{aligned} \tag{9}$$

In equations (9) the mixture-averaged approximation for species diffusion is obtained from the multicomponent formulation by deleting the terms containing sums over the ordinary diffusion fluxes and using the mixture-averaged form of D_{km}, equation (8).

The viscosity of the mixture is obtained from a gas-phase transport properties software package [5] that is used in conjunction with the chemical kinetics software, CHEMKIN (Kee *et al.* [6]); the formulation is the semi-empirical formula of Wilke [7], modified by Bird *et al.* [8]. Kinetic theory expressions (Hirschfelder *et al.* [9]) are used for the pure species viscosities. The mixture is assumed to be composed of ideal gases, and the low Mach number approximation has been made (Paolucci [10]), i.e. the pressure, P^*, is assumed to be constant in the equation of state: $P^*=\rho^*R^*T^*/M^*$, and the dynamic pressure, p_m, is determined by solving an equation that satisfies mixture mass conservation. In dimensionless form, the equation of state is: $\rho=M/(1+\varepsilon T)$ where $\varepsilon=(T^*_{\max}-T^*_{\mathrm{ref}})/T^*_{\mathrm{ref}}$ and for isothermal flow ($\varepsilon=0$) considered in this study, $\rho=M$.

The dimensionless parameters in the above equa-

tions are the Reynolds number $Re = u^*_{\text{ref}} D^* / \nu^*_{\text{ref}}$, the Froude number $Fr = u^{*2}_{\text{ref}}/(g^* D^*)$, the Schmidt numbers $Sc_{km} = \nu^*_{\text{ref}}/D^*_{km\,\text{ref}}$, $k = 1, \ldots, K$, and the dimensionless properties: $\rho = \rho^*/\rho^*_{\text{ref}}$, $\mu = \mu^*/\mu^*_{\text{ref}}$, $D_{km} = D^*_{km}/D^*_{km\,\text{ref}}$, $M = M^*/M^*_{\text{ref}}$, and $\mathfrak{D}_{ik} = \mathfrak{D}^*_{ik}/D^*_{km\,\text{ref}}$.

The inlet boundary conditions are the specified mixture flow rate, Q^*_{ref}; temperature, T^*_{ref}; composition, $X_{SiF_4}|_{(x=0^-)}$ and $X_{NH_3}|_{(x=0^-)}$, with the products HF, N_2, and H_2 equal to zero at $x = 0^-$. The mixture is assumed to enter the tube with a parabolic velocity distribution. At the outflow boundary ($x = 1.5$), the usual zero x derivative conditions are applied on all dependent variables.

SURFACE CHEMISTRY

Larson [11] has developed a one-dimensional model of the UTRC Si_3N_4 process and used the model to obtain the surface chemistry rate expressions by fitting to an experimental database [1]. The model allows for both crystalline and amorphous deposition of Si_3N_4 on the surface as well as the surface decomposition of NH_3 to account for the observed presence of H_2 in the reactor. In the present study, the temperatures considered are sufficiently high that only crystalline deposition is assumed in the overall surface reactions:

$$3SiF_4 + 4NH_3 \xrightarrow{r_1^*} Si_3N_4\,(s) + 12HF$$

$$2NH_3 \xrightarrow{r_2^*} N_2 + 3H_2$$

where

$$r_1^* = r^*_{1\,\text{ref}} r_1, \quad r_2^* = r^*_{2\,\text{ref}} r_2$$

with

$$r_1 = \exp\left[E_1^*/R^*(1/T^*_{\text{ref}} - 1/T^*)\right] X_{SiF_4} X_{NH_3} \tag{10}$$

and

$$r_2 = \exp\left[E_2^*/R^*(1/T^*_{\text{ref}} - 1/T^*)\right] X_{NH_3} \tag{11}$$

$$E_1^* = 132.9\ \text{kcal mol}^{-1},$$

$$E_2^* = 54.8\ \text{kcal mol}^{-1},$$

$$R^* = 1.987 \times 10^{-3}\ \text{kcal mol}^{-1}\,\text{K}^{-1}$$

$$r^*_{1\,\text{ref}} = 1.8123 \times 10^{11} \exp\left[-E_1^*/(R^* T^*_{\text{ref}})\right]$$

$$\text{moles Si}_3\text{N}_4\ \text{cm}^{-2}\,\text{s}^{-1}$$

$$r^*_{2\,\text{ref}} = 1.1195 \times 10^{1} \exp\left[-E_2^*/(R^* T^*_{\text{ref}})\right]$$

$$\text{moles N}_2\ \text{cm}^{-2}\,\text{s}^{-1}.$$

The boundary conditions at a deposition surface for each gas phase species k relate the mass flux of species k at the surface to its production/destruction rate by surface chemical reaction:

$$(\rho_k^* \mathbf{v}_k^* \cdot \mathbf{n})_s = \sum_{\alpha=1}^{2} \nu_{k\alpha} r_\alpha^* M_k^*, \quad k = 1, \ldots, (K-1)$$

where $\nu_{k\alpha}$ is the stoichiometric coefficient for species k in surface reaction α; it is positive for gas phase species on the left side of the reaction expression and negative for gas phase species on the right side.

In dimensionless form,

$$(\rho_k \mathbf{v}_k \cdot \mathbf{n})_s = \frac{1}{Re} \sum_{\alpha=1}^{2} \frac{Da_{km\alpha}}{Sc_{km}} r_\alpha M_k, \quad k = 1, \ldots, (K-1). \tag{12}$$

The surface Damkohler numbers relate the time scale for mass diffusion of species k to the time scale for surface chemical reaction of species k:

$$Da_{km_\alpha} = \frac{\nu_{k\alpha} r^*_{\alpha\,\text{ref}} M^*_{\text{ref}} D^*}{\rho^*_{\text{ref}} D^*_{km\,\text{ref}}}.$$

Summing over all species in the gas phase gives the bulk velocity at a reacting surface (the boundary conditions for the momentum equations):

$$(\rho \mathbf{v} \cdot \mathbf{n})_s = \frac{1}{Re} \sum_{k=1}^{K} \sum_{\alpha=1}^{2} \frac{Da_{km\alpha}}{Sc_{km}} r_\alpha M_k. \tag{13}$$

Note that equation (12) can be written as the sum of two parts:

$$(\rho_k \mathbf{v}_k \cdot \mathbf{n})_s = (\rho Y_k \mathbf{v} \cdot \mathbf{n})_s + \frac{1}{Re \cdot Sc_{km}} \mathbf{j}_k^v \cdot \mathbf{n}_s,$$

where the first term on the right hand side is the dimensionless mass flux of species k at the surface due to the bulk flow, and the second term is the flux at the surface due to the diffusion of species k. The study includes the five gas-phase species: SiF_4, NH_3, HF, H_2, and N_2 and the above two surface reactions.

NUMERICAL SOLUTION

Methodology

The conservation equations (1)–(3), (9) are transformed to a generalized coordinate system in a manner similar to that discussed in Shyy *et al.* [12] to allow solutions in an arbitrary axisymmetric geometry. The transformed equations are integrated over control volumes and discretized using either central differences for all remaining derivatives or the hybrid differencing scheme (Patankar [13]). The transformed, control volume form of the mixture continuity equation is used in the SIMPLER method to determine the pressure, p_m. In this study we are interested in the steady-state behavior of the process; the transient term was effectively removed from the equations by taking a single very large (10^{20}) time step.

A sequential line by line relaxation scheme is used to solve the discretized equations and boundary conditions discussed above. Four of the five species conservation equations are solved; the specific species actually solved depend on the method used for determining the species diffusion. For multicomponent diffusion, N_2 was the species that was not solved. For the approximate mixture-averaged formulation of species diffusion, either NH_3 or N_2 was the species not solved. The $K-1$ independent equations (5) for the

species mass diffusion fluxes, along with the requirement that $\Sigma_1^K \mathbf{j}_k^c = \mathbf{0}$, are solved directly at each iteration for the K unknown fluxes in the multicomponent formulation.

Convergence criteria

An iterative method is used to solve the coupled, nonlinear set of equations. Underrelaxation factors (typical values were 0.5) are used for the momentum and species mass conservation equations to avoid numerical instabilities; no underrelaxation was applied to the pressure equation. Iterations were continued until changes in the deposition rate and mass diffusion fluxes for all species were less than 1–2%, where this variation was calculated over an interval of several thousand global iterations. Convergence for the above quantities was the slowest of all the results examined and had the most impact on the final results. Typically, 25 000–35 000 iterations were required to obtain convergence; computational times were several hours on a CRAY-YMP. Usually, restarts from previously converged results were selected as initial conditions for a new case. A global mass balance that accounted for the mass lost due to deposition on the tube surface was monitored and was maintained to within 1.0%. For the nominal conditions cited below, 13% of the mass entering the tube was deposited on the tube surface.

Grid sensitivity

Most of the results discussed below were obtained on a nonuniform grid of 70 by 35 control volumes in the x and r directions, respectively, with the finer grid spacings near the start of the reacting region ($x = 0.75$) and the tube surface ($r = 0.5$). Some calculations were also made on a nonuniform x, r grid of 50 by 25. Results from the case for the nominal conditions were compared using these two grid resolutions. Deposition rate profiles and contours of species mole fractions for the two grids differed by less than 1%; similar small differences occurred in the individual species mass diffusion fluxes at a location near the inlet of the tube.

RESULTS

Unless otherwise noted, the results presented and discussed here are for the multicomponent formulation of species diffusion. The nominal conditions studied are: $T^*_{\text{ref}} = T^* = T = 1713$ K (isothermal flow), $Q^*_{\text{ref}} = 688$ sccm, $P^* = 1.8$ Torr, inlet reactant molar ratio of 6:1 ($[X_{NH_3}/X_{SiF_4}]|_{x=0} = 6$), and tube diameter, $D^* = 13.34$ cm. These values result in values of Fr and Re of 3.6 and 2.5, respectively. Table 1 provides a compilation of the cases reported along with the maximum, minimum, average, and percent variation in the deposition rates on the reacting section of the tube. We note that the maximum deposition rate occurs at the leading edge of the reacting section of the tube; the deposition rate falls monotonically in the downstream direction with considerable variation for the cases studied.

To compare the relative effects of convection, $\rho_k^* \mathbf{u}^*$, and diffusion, $\mathbf{j}_k^{c^*}$, of species k, we divide by the reference dimensional quantities ρ^*_{ref} and u^*_{ref} and obtain the dimensionless quantities, $\rho_k \mathbf{u}$ and $j_k/(Re \cdot Sc_{km})$. These are presented as vectors with filled (convection) and unfilled (diffusion) arrowheads. For comparison and reference among figures, we show an arrow, the length of which represents the dimensionless reference mass flux of the mixture: $\rho^*_{\text{ref}} u^*_{\text{ref}} / \rho^*_{\text{ref}} u^*_{\text{ref}} = 1$.

Effects of flow rate

The effect of flow rate on the convective and diffusive mass fluxes of species HF is shown in Fig. 2. We focus on HF because it is generally representative of species behavior in the system, although other species do exhibit differences, e.g. the large diffusion of H_2. Being a gaseous product of the surface deposition reaction, HF is produced along the surface of the tube beginning at $x = 0.75$; for the high flow rate of 6880

Table 1. Deposition rate of Si_3N_4 on tube surface

T^* (K)	Q^* (sccm)	NH_3/SiF_4 molar ratio	Diffusion model	Grid	Maximum deposition rate (μ h^{-1})	Minimum deposition rate (μ h^{-1})	Average deposition rate (μ h^{-1})	Variation in deposition rate (%)
1713	688	6:1	mult.	70×35	107.0	33.9	51.7	68.3
1713	6880	6:1	mult.	70×35	242.0	115.0	146.8	52.4
1783	688	6:1	mult.	70×35	229.5	35.2	72.5	84.6
1783	6880	6:1	mult.	70×35	645.4	179.3	264.8	72.2
1643	688	6:1	mix. avg.†	50×25	37.9	22.6	27.0	40.3
1643	6880	6:1	mix. avg.†	50×25	61.6	45.8	50.8	25.7
1713	688	3:1	mix. avg.†	70×35	170.3	56.3	84.5	66.9
1713	688	6:1	mix. avg.†	70×35	114.7	37.5	56.8	67.3
1713	688	6:1	mix. avg.†	50×25	112.9	37.4	56.2	66.9
1713	6880	6:1	mix. avg.‡	70×35	242.5	115.0	146.8	52.6

† Did not solve species conservation equation for Y_{N_2}.
‡ Did not solve species conservation equation for Y_{NH_3}.

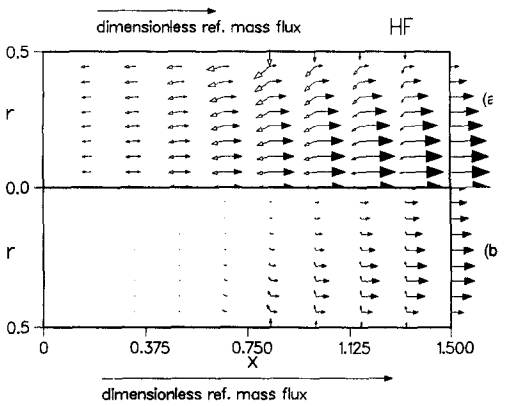

FIG. 2. Arrows representing the dimensionless convection and diffusion mass fluxes of HF for $T = 1713$ K, 6 : 1 molar ratio of NH_3 to SiF_4: (a) 688 sccm; (b) 6880 sccm.

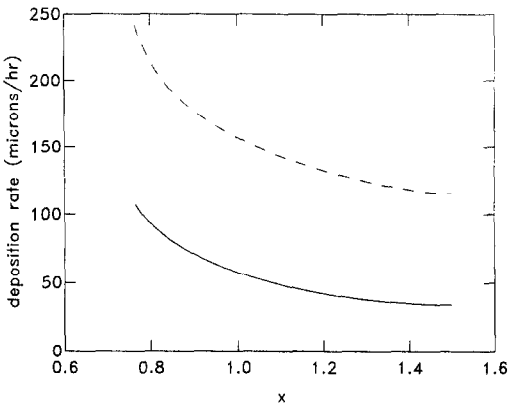

FIG. 4. Deposition rate of Si_3N_4 along the reacting surface of the tube for $T = 1713$ K, 6 : 1 molar ratio of NH_3 to SiF_4: (——) 688 sccm; (– – –) 6880 sccm.

sccm ($Re = 25.3$) in Fig. 2(b) there is little diffusive flux of HF in the upstream region of the tube. In the reaction region HF diffuses away from the surface where it is produced. At the lower flow rate of 688 sccm ($Re = 2.53$) in Fig. 2(a), there is a significant diffusive flux of HF even for $x < 0.75$. Comparing the fluxes at the two flow rates, we note that the parabolic radial distribution of the HF convective mass flux at the lower flow rate is similar to the radial distribution of the convective mass flux of the mixture (not shown), whereas for the higher flow rate the HF convective flux has a maximum at a radial position between the reacting surface and the tube centerline. At the higher flow rate the HF generated at the surface is primarily swept downstream and cannot diffuse to the tube centerline as readily as it can at the lower flow rate (cf. Figs. 2 and 3).

The effects of flow rate on the mole fraction contours of HF and the Si_3N_4 deposition rate are shown in Figs. 3 and 4, respectively, for $T = 1713$ K. At the higher flow rate of 6880 sccm ($Re = 25.3$) shown in Fig. 3(b), a concentration boundary layer forms starting near the beginning ($x = 0.75$) of the reacting surface section with little upstream diffusive effects. At the lower flow rate of 688 sccm ($Re = 2.53$, Fig. 3(a)), there are strong diffusive effects. Since the Schmidt number for HF ($Sc_{HF,m}$) is 0.6, the Peclet number for mass transfer, $Pe_{HF,m} = Re \cdot Sc_{HF,m} = u^*_{ref}D^*/D^*_{HF,m\,ref} = 1.5$, a value that shows convection and diffusion to be of approximate equal magnitudes, resulting in the upstream diffusion. At the higher flow rate, $Pe_{HF,m} = 15$, which, as noted above, yields little upstream diffusion. The relatively uniform contours in the radial direction for the lower flow rate in Fig. 3(a) are another indicator of significant diffusion for these conditions.

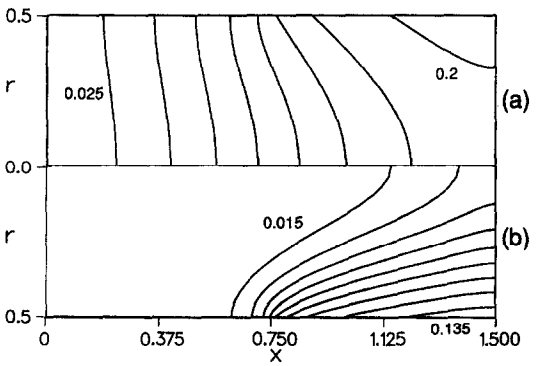

FIG. 3. HF molar fraction contours for $T = 1713$ K, 6 : 1 molar ratio of NH_3 to SiF_4: (a) 688 sccm, minimum 0.025, maximum 0.2, increment 0.025; (b) 6880 sccm, minimum 0.015, maximum 0.135, increment 0.015.

The surface chemical reaction (equation (10)) consumes SiF_4 starting at $x = 0.75$; however, for the lower flow rate case the mole fraction of SiF_4 (not shown) is reduced below its inlet value of 0.143 at locations upstream of the start of the surface reacting region. This reduction is significant, and, since the surface reaction rate depends on the concentration of SiF_4 at the surface, the deposition rate is decreased for the lower flow rate. The deposition rates of Si_3N_4 along the tube surface are shown in Fig. 4 for the two flow rates 688 and 6880 sccm. The deposition rates are highly nonuniform, and increasing the flow rate by an order of magnitude results in a decrease in nonuniformity of only 15% (from 68 to 53%). For $T = 1713$ K, the surface Damkohler number for SiF_4 is 1.1, indicating that the time scales for deposition chemistry and diffusion are approximately equal. For both flow rates, reactant depletion occurs (not shown but similar to the spatial variation of the product HF contours of Fig. 3) although it is small at the higher flow rate. Consequently the variation of the deposition rate with position along the tube results from both depletion and dilution of the reactants and growth (from $x = 0.75$ to 1.5) of the concentration boundary layers.

Effects of temperature

The effect of increasing the temperature (and hence the surface chemical reaction rates) from 1713 to 1783 K on the transport and deposition is shown in Figs.

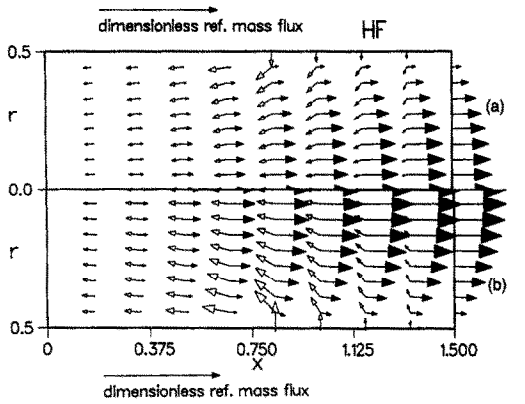

FIG. 5. Arrows representing the dimensionless convection and diffusion mass fluxes of HF for 688 sccm, 6:1 molar ratio of NH_3 to SiF_4: (a) $T = 1713$ K; (b) $T = 1783$ K.

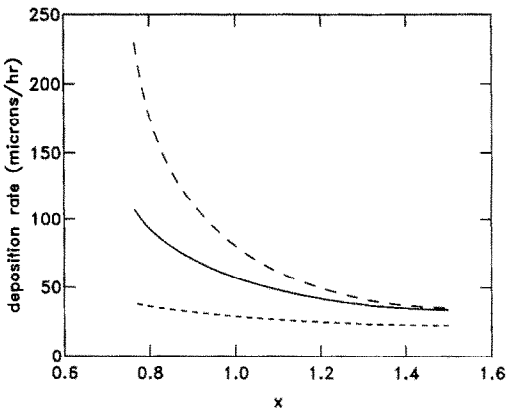

FIG. 7. Deposition rate of Si_3N_4 along the reacting surface of the tube for 688 sccm, 6:1 molar ratio of NH_3 to SiF_4: (——) $T = 1713$ K; (– – –) $T = 1783$ K; (----) $T = 1643$ K.

5–7. Comparing Figs. 5(b) and (a) there is enhanced convection and diffusion of HF due to the increased amounts of HF present in the mixture at the higher temperature. Figures 6(a) and (b) show the HF mole fraction contours at 1713 and 1783 K, respectively. In Fig. 6(b), the HF mole fraction has increased to 25% of the mixture in the downstream region. The deposition rates of Si_3N_4 at the three temperatures studied are shown in Fig. 7. The deposition rate is significantly higher at 1783 K than at 1713 K, and is very nonuniform, the initial rate (at $x = 0.75$) decreasing by 84% over the reacting region. The surface Damkohler number for SiF_4 is now 5.1; reactant depletion is significant with the SiF_4 mole fraction (not shown) less than 0.03 at the downstream end of the reacting region. The effects of increasing the flow rate from 688 to 6880 sccm at 1783 K (not shown) are similar to those at 1713 K shown in Figs. 2–4.

The effect of reducing the temperature (and hence the surface chemical reaction rates) to 1643 K on the transport and deposition is shown in Figs. 7–9. At the lower temperature of 1643 K there is reduced diffusion and convection of HF compared with that at 1713 K. This is due to the reduced amount of HF being formed as shown in the comparison of Figs. 9(a) and (b), where in Fig. 9(b) HF only accounts for about 10% of the mixture by mole fraction in the downstream region. The deposition rate on the surface of the tube is now significantly lower and more uniform; the initial deposition rate of 38 microns h^{-1} decreases by 40% by the end of the reacting region. The surface Damkohler number for SiF_4 is now 0.4. The results shown in Figs. 7–9 for 1643 K were computed on a 50 by 25 (x,r) grid and are for the mixture-averaged formulation of diffusion. Again, the effects of increasing the flow rate from 688 to 6880 sccm at 1643 K (not shown) are similar to those at 1713 K shown in Figs. 2–4.

Although the deposition uniformity is improved at lower temperature (smaller Damkohler number), the magnitude of the deposition rate is reduced (cf. Fig. 7). The nonuniformity in deposition rate is reduced somewhat as shown in Fig. 4 with a higher flow rate (larger Reynolds number). We note that the morphology of deposited Si_3N_4 changes from crystalline to amorphous at a reaction temperature around 1650 K. Kinetic expressions for the low temperature amorphous deposition of Si_3N_4 have been obtained by Larson [11].

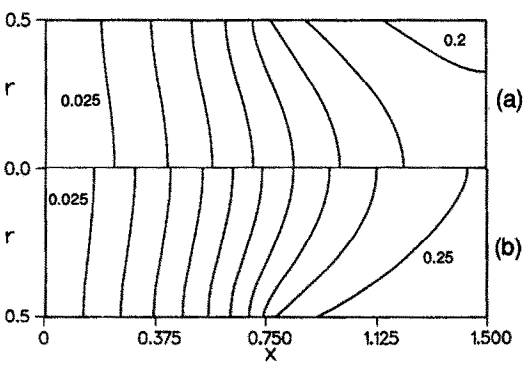

FIG. 6. HF molar fraction contours for 688 sccm, 6:1 molar ratio of NH_3 to SiF_4: (a) $T = 1713$ K, minimum 0.025, maximum 0.2, increment 0.025; (b) $T = 1783$ K, minimum 0.025, maximum 0.25, increment 0.025.

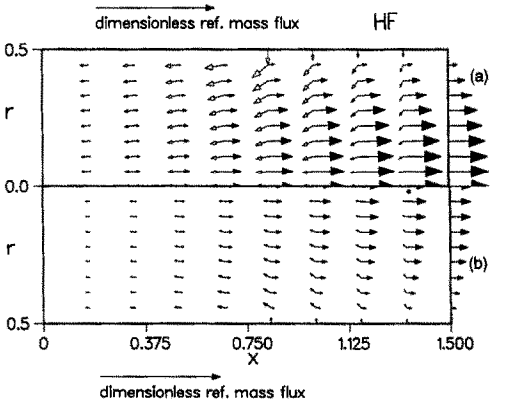

FIG. 8. Arrows representing the dimensionless convection and diffusion mass fluxes of HF for 688 sccm, 6:1 molar ratio of NH_3 to SiF_4: (a) $T = 1713$ K; (b) $T = 1643$ K.

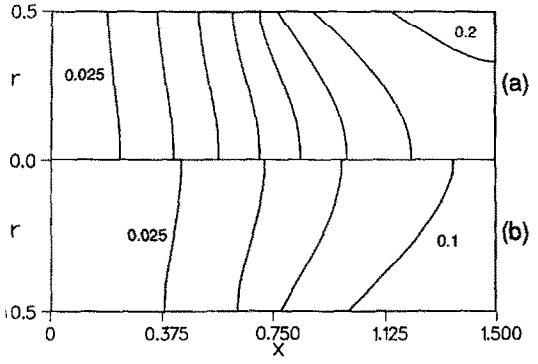

FIG. 9. HF molar fraction contours for 688 sccm, 6 : 1 molar ratio of NH_3 to SiF_4: (a) $T = 1713$ K, minimum 0.025, maximum 0.2, increment 0.025; (b) $T = 1643$ K, minimum 0.025, maximum 0.1, increment 0.025.

Effects of reactant mole ratio

Figure 10 shows the deposition rate at the conditions: flow rate 688 sccm, temperature 1713 K, for two values of the inlet mole ratio: 6 : 1 and 3 : 1 (NH_3 to SiF_4). For the smaller molar ratio case, the Damkohler number is increased to 3 from its value of 1.1 at the larger molar ratio case, resulting in a significantly higher value of the deposition rate. Due to the increased mixture density at the smaller molar ratio, the mass flow rate is larger ($Re = 3.2$) than for the nominal case ($Re = 2.5$), resulting in deposition nonuniformity approximately equal to that for the nominal case. The results at molar ratio 3 : 1 were computed using a 70 by 35 (x,r) grid and the mixture-averaged formulation for diffusion.

Effects of diffusion formulation

The mixture-averaged formulation of diffusion is approximate and becomes more accurate when solving for dilute species. Usually the implementation of the mixture-averaged formulation (see Kee *et al.* [5]) involves the solution of $K-1$ species conservation equations (K = total number of species), with the remaining species mass fraction obtained from $\Sigma_1^K Y_k = 1$. If one species dominates, then the conservation equations for the other species can be solved and the largest one obtained from the above summation. If there is no dominant species globally, this procedure can be implemented on a local basis.

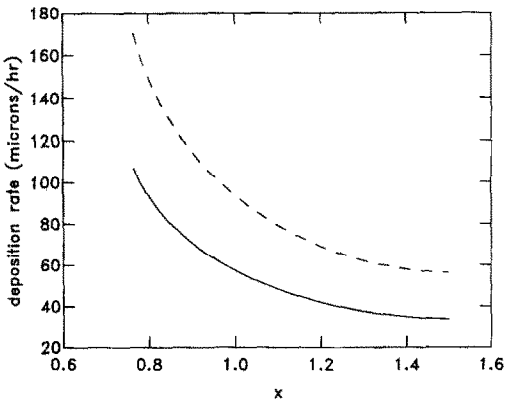

FIG. 10. Deposition rate of Si_3N_4 along the reacting surface of the tube for 688 sccm, 6 : 1 molar ratio of NH_3 to SiF_4: (——) $T = 1713$ K; (– – –) $T = 1643$ K.

Comparisons were made using both multicomponent and mixture-averaged formulations for several cases. NH_3 is the dominant species in most situations and over much of the domain. In the mixture-averaged formulation the conservation equations for the other species (SiF_4, HF, H_2, and N_2) were solved and Y_{NH_3} was obtained from $\Sigma_1^K Y_k = 1$. For the case of 1713 K, 6880 sccm, and 6 : 1 molar ratio of NH_3 to SiF_4, agreement for all species concentrations and the deposition rate obtained from both formulations are very good (not shown). We caution that the validity of this procedure has not been established for all conditions in this study.

We have also investigated the case when the conservation equation for the dominant species, i.e. NH_3, is solved, and Y_{N_2} is then obtained from the above summation. For this case, there is again good agreement for the four species that are determined from conservation equations. However, for Y_{N_2} there is now marked disagreement. In view of the small mole fraction of N_2 (maximum value of 0.06), the resulting error in the N_2 concentration using the mixture-averaged formulation and not solving the conservation equation for this species might be expected.

SUMMARY AND CONCLUSIONS

Numerical solutions of the mixture continuity, Navier–Stokes, and species mass conservation equations with multicomponent diffusion have been obtained to predict the flow field, species distributions, and deposition rates in a cylindrical hot-wall, low-pressure CVD reactor for the deposition of Si_3N_4 from SiF_4 and NH_3.

The relative effects of diffusion, convection, and surface chemistry for these low-pressure CVD conditions have been determined over a range of the system operating parameters. There is significant depletion of reactants; species diffusion is important, and, except for the high flow rate conditions, significant upstream diffusion occurs and results in dilution of the reactants. The deposition rate of Si_3N_4 is highly nonuniform except at the lowest temperature studied. Results have been compared using an approximate mixture-averaged formulation for the species diffusion to those from the multicomponent formulation. For the conditions compared, agreement is good for all species if, when using the mixture-averaged formulation, the conservation equation for the dominant species, NH_3, is not solved. If N_2, a nondominant species, is not solved in the mixture-averaged approach, then the agreement with the multicomponent formulation is not good for that species but is reasonably good for the other species.

Acknowledgements—The authors would like to thank the following people for many valuable discussions, suggestions, and information during the course of this study: Rich Larson, Bob Kee, Pauline Ho, Woo Lee, Dick Veltri, and Jim Strife. Thanks to Bill Winters for developing code interfaces to mesh generation and post processing codes. We acknowledge the use of AP, a mesh generation and post-processing code developed by Ken Perano, Paul Nielan, and Bill Mason. This work was supported by the U.S. Department of Defense (DARPA-DSO) under Air Force Wright Laboratory (AFWL) Contract F33615-89-C-5628. The DARPA sponsor was William Barker, and the AFWL monitor was Joseph Hager.

REFERENCES

1. W. Y. Lee, J. R. Strife and R. D. Veltri, Low pressure chemical vapor deposition of α-Si_3N_4 from SiF_4 and NH_3: kinetic characteristics, *J. Am. Ceram. Soc.* **75,** 2200–2206 (1992).
2. P. Ho and M. E. Coltrin, Sandia National Laboratories, unpublished data.
3. C. Kleijn, Transport phenomena in chemical vapor deposition reactors, p. 23. PhD Thesis, Delft University of Technology, The Netherlands (1991).
4. C. F. Curtiss and J. O. Hirschfelder, Transport properties of multicomponent gas mixtures, *J. Chem. Phys.* **17,** 550–555 (1949).
5. R. J. Kee, G. Dixon-Lewis, J. Warnatz, M. E. Coltrin and J. A. Miller, A Fortran computer code package for the evaluation of gas-phase multicomponent transport properties, Sandia Report SAND86-8246 (1986).
6. R. J. Kee, F. M. Rupley and J. A. Miller, CHEMKIN-II: a fortran chemical kinetics package for the analysis of gas-phase chemical kinetics, Sandia Report SAND89-8009 (1989).
7. C. R. Wilke, A viscosity equation for gas mixtures, *J. Chem. Phys.* **18,** 517 (1950).
8. R. B. Bird, W. E. Stewart and E. N. Lightfoot, *Transport Phenomena*, p. 258. Wiley, New York (1960).
9. J. O. Hirschfelder, C. F. Curtiss and R. B. Bird, *Molecular Theory of Gases and Liquids*. Wiley, New York (1954).
10. S. Paolucci, On the filtering of sound from the Navier–Stokes equations, Sandia Report SAND82-8257 (1982).
11. R. S. Larson, Kinetics of silicon nitride chemical vapor deposition from SiF_4 and NH_3. *J. Am. Ceram. Soc.* **76,** 1930–1936 (1993).
12. W. Shyy, S. S. Tong and S. M. Correa, Numerical recirculating flow calculation using a body-fitted coordinate system, *Numer. Heat Transfer* **8,** 99–113 (1985).
13. S. V. Patankar, *Numerical Heat Transfer and Fluid Flow*. McGraw-Hill, New York (1980).